

# Signatures of leptophilic t-channel dark matter from active galactic nuclei

Marina Cermeño Gavilán

Centre for Cosmology, Particle Physics and Phenomenology (CP3),  
Université Catholique de Louvain, Belgium.

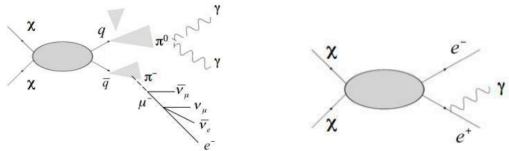
Based on

M. Cermeño, C. Degrande, L. Mantani, PRD 105 (2022) 8, 083019, arXiv: 2201.07247

May 24, 2022



# Indirect photon signals of dark matter (DM)



$$\frac{d\Phi}{dE_\gamma}(E_\gamma, \Delta\Omega_{\text{obs}}) = \frac{\langle\sigma v\rangle}{8\pi m_\chi^2} \frac{dN}{dE_\gamma}(E_\gamma) \int_{\Delta\Omega_{\text{obs}}} d\Omega \int_{\text{l.o.s}} ds \rho_{DM}^2(r(s, \theta))$$

- $\langle\sigma v\rangle$  averaged annihilation cross section of DM particles of mass  $m_\chi$
- $\frac{dN}{dE_\gamma}(E_\gamma)$  energy spectrum per annihilation event,  $E_\gamma$  photon energy
- $\rho_{DM}(r)$  DM density profile,  
 $r^2 = s^2 + r_0^2 - 2r_0 s \cos\theta$ ,  $r_0$  radial distance from the observer to the target
- $\Delta\Omega_{\text{obs}}$  solid angle of observation

# DM density in some active galactic nuclei

Adiabatic growth of a super-massive black hole in a region with an initial DM distribution

$$\rho_{\text{DM}}^0(r) \propto \rho_0 (r/r_0)^{-\gamma} \Rightarrow \text{DM spike formation}$$
 Gondolo, Silk, PRL 83 (1999) 1719

$$\rho_{\text{DM}}(r) = \begin{cases} 0 & r < 4R_S \\ \frac{\rho_{\text{sp}}(r)\rho_{\text{sat}}}{\rho_{\text{sp}}(r)+\rho_{\text{sat}}} & 4R_S \leq r < R_{\text{sp}}, \\ \rho_0 \left(\frac{r}{r_0}\right)^{-\gamma} \left(1 + \frac{r}{r_0}\right)^{-2} & r \geq R_{\text{sp}} \end{cases}$$

- $R_S = 5 \times 10^{-6}$  pc the Schwarzschild radius
- $R_{\text{sp}} = \alpha_\gamma r_0 \left(\frac{M_{\text{BH}}}{\rho_0 r_0^3}\right)^{1/(3-\gamma)}$  the spike radius, with  $\alpha_\gamma$  a normalization constant that depends on  $\gamma$  and can be obtained numerically
- The spike distribution

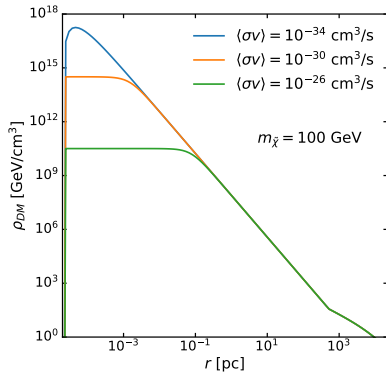
$$\rho_{\text{sp}}(r) = \rho_R g_\gamma(r) \left(\frac{R_{\text{sp}}}{r}\right)^{\gamma_{\text{sp}}}, \quad \rho_R = \rho_0 \left(\frac{R_{\text{sp}}}{r_0}\right)^{-\gamma}, \quad g_\gamma(r) \simeq \left(1 - \frac{4R_S}{r}\right)^3, \quad \gamma_{\text{sp}} = \frac{9 - 2\gamma}{4 - \gamma}$$

- The maximum density allowed by DM annihilations,  $\rho_{\text{sat}} \simeq \frac{m_\chi}{\langle\sigma v\rangle t_{\text{BH}}}$ , during  $t_{\text{BH}} \sim 10^{10}$  yr
- We take  $\gamma = 1$ , NFW profile for  $r \geq R_{\text{sp}}$  and  $\gamma_{\text{sp}} = 7/3$

# DM density in Cen A

$$\rho_{DM}(r) = \begin{cases} 0 & r < 4R_S \\ \frac{\rho_{sp}(r)\rho_{sat}}{\rho_{sp}(r)+\rho_{sat}} & 4R_S \leq r < R_{sp} \\ \rho_0 \left(\frac{r}{r_0}\right)^{-1} \left(1 + \frac{r}{r_0}\right)^{-2} & r \geq R_{sp} \end{cases}$$
$$\rho_{sp}(r) = \rho_0 \left(\frac{R_{sp}}{r_0}\right)^{-1} \left(1 - \frac{4R_S}{r}\right)^3 \left(\frac{R_{sp}}{r}\right)^{7/3},$$
$$\rho_{sat} \simeq \frac{m_\chi}{\langle\sigma v\rangle t_{BH}}$$

with  $R_S = 5 \times 10^{-6}$  pc,  $r_0 = 20$  kpc,  $\rho_0 \sim 1$  GeV/cm<sup>3</sup>,  $R_{sp} = 10^8 R_S$



M. Cermeño, C. Degrande, L. Mantani, PRD 105 (2022) 8, 083019, arXiv: 2201.07247

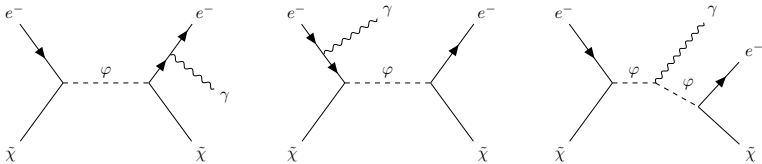
# The model

$$\mathcal{L}_{DM} = i\bar{\psi}_{\tilde{\chi}}(\not{D} - m_{\tilde{\chi}})\psi_{\tilde{\chi}} + D_\mu\varphi^\dagger D^\mu\varphi - m_\varphi\varphi^\dagger\varphi + (a_R \bar{e}_R \psi_{\tilde{\chi}} \varphi + h.c.).$$

Bringmann et al., JCAP 07 (2012) 054, Garny et al., JCAP 12 (2013) 640, Kopp, Michaels, Smirnov, JCAP 04 (2014) 022, Okada, Toma, PLB 750 (2015) 266, Garny, Ibarra, Vogl, Int.J.Mod.Phys.D 24 (2015) 07, 1530019

$\tilde{\chi}$  Majorana fermion,  $\varphi$  charged scalar mediator,  $e_R$  right-handed electrons

- $m_\varphi \gtrsim m_{\tilde{\chi}}$  and  $\Delta M = m_\varphi - m_{\tilde{\chi}} \ll m_\varphi, m_{\tilde{\chi}}$
- $\tilde{\chi}\tilde{\chi} \rightarrow e^+e^-$  velocity suppressed
- Relevant annihilation channels  $\tilde{\chi}\tilde{\chi} \rightarrow \gamma\gamma, \tilde{\chi}\tilde{\chi} \rightarrow e^-e^+\gamma \Rightarrow$  line-like signatures
- Resonantly enhanced DM scattering off electrons in the AGN jet



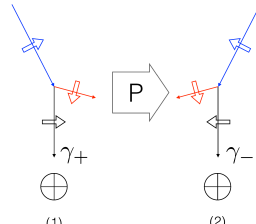
# Circular polarised photons

- A net circular polarisation signal is generated when there is an excess of one photon polarisation state over the other
- Parity must be violated in at least one of the dominant photon emission processes

$$\mathcal{A}_- \neq \mathcal{A}_+$$

$$\mathcal{A}_\pm = \sum_{spins} |\epsilon_\pm^\mu M_{\mu l}|^2$$

$$\epsilon_\pm^\mu(k) = \frac{1}{2}(\mp \epsilon_1^\mu(k) - i \epsilon_2^\mu(k))$$



*Boehm et al., JCAP 05 (2017) 043*

- There must be an asymmetry in the number density of one of the particles in the initial state or CP must be violated
- A P violating interaction like  $e^- \tilde{\chi} \rightarrow e^- \tilde{\chi} \gamma$  in a region with an abundance of electrons over positrons → circularly polarised photons *Boehm et al. JCAP 05 (2017) 043*  
The circular polarisation asymmetry can reach 90 % for interactions in the GC  
*M. Cermeño, C. Degrande, L. Mantani, Phys. Dark Univ. 34 (2021) 100909*
- No net polarisation from  $\tilde{\chi} \tilde{\chi} \rightarrow e^- e^+ \gamma$ , initial state is a CP-eigenstate

# Circular polarised photon flux from Cen A

The flux of circularly polarised photons from  $e^-\tilde{\chi} \rightarrow e^-\tilde{\chi} \gamma_\pm$  at  $d_{\text{AGN}} \sim 3.8 \text{ Mpc}$

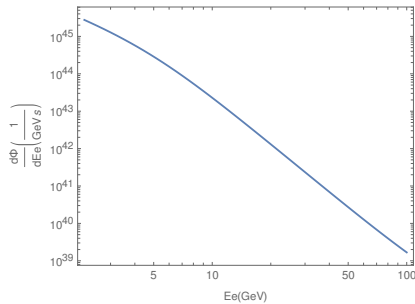
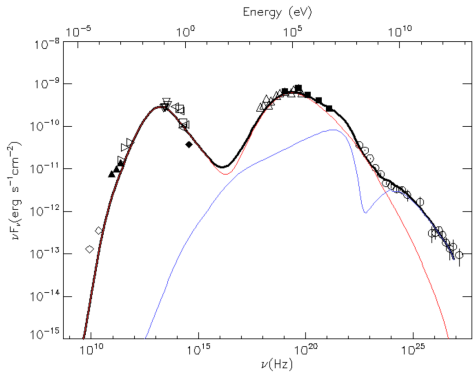
M. Cermeño, C. Degrande, L. Mantani, PRD 105 (2022) 8, 083019, arXiv: 2201.07247

$$\frac{d\Phi_{\gamma,pol}}{dE_\gamma} = \frac{1}{d_{\text{AGN}}^2} \frac{\delta_{DM}}{m_\chi} \int dE_e \frac{d\Phi_e^{\text{AGN}}}{dE_e} \left| \frac{d^2\sigma_+}{dE_\gamma d\Omega_\gamma}(E_e, E_\gamma, \theta_0) - \frac{d^2\sigma_-}{dE_\gamma d\Omega_\gamma}(E_e, E_\gamma, \theta_0) \right|$$

- $\delta_{DM} \equiv \int_{r_{min}}^{r_0} \rho_{DM}(r) dr$  the integral of the DM density along the direction of the jet  
 $r_{min}$  minimum distance from the AGN center at which the scattering takes place  
 $r_0$  the distance at which the AGN jet fades
- $\frac{d^2\sigma_\pm}{dE_\gamma d\Omega_\gamma}(E_e, E_\gamma, \theta_0)$  the differential cross section for  $e^-\tilde{\chi} \rightarrow e^-\tilde{\chi} \gamma_\pm$ , with  $\Omega_\gamma$  the solid angle between the emitted photon and the incoming electron.  
The polar coordinate  $\theta_\gamma$  is fixed at  $\theta_0$ , angle between the position of the AGN jet of electrons with respect the line of sight
- $\frac{d\Phi_e^{\text{AGN}}}{dE_e}$  the electron energy spectrum in units of  $\text{erg}^{-1} \text{ s}^{-1}$

# The electron energy spectrum in the jet

Assuming that the gamma-ray photons coming from the Cen A core are due to synchrotron self-Compton radiation from two emitting zones (both located at  $\theta_0 = 30^\circ$  with respect to the line of sight), the electron energy spectrum can be derived [Abdalla et al., A & A 619 \(2018\) A71](#)

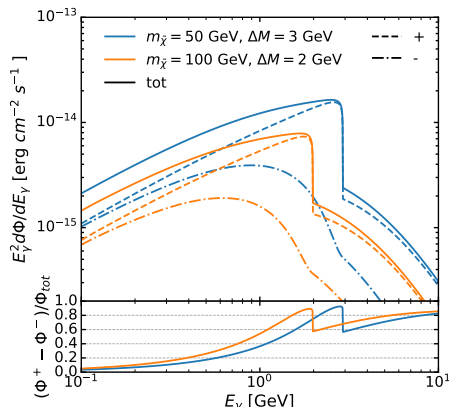
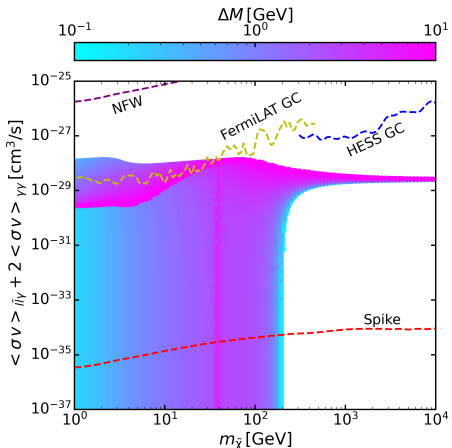


We use this photon flux as our background to measure the signals and to put constraints

# Exclusion from annihilation and circular polarised flux

- Allowed DM candidates  $m_{\tilde{\chi}} \sim 40 - 200$  GeV and  $a_R \lesssim 10^{-2}$
- $\Delta M$  for the survived parameter space points fixed by the relic density and span from  $\Delta M = 3(1)$  GeV for  $m_{\tilde{\chi}} = 50(200)$  GeV

M. Cermeño, C. Degrande, L. Mantani, PRD 105 (2022) 083019



Asymmetries close to 100 %

Sensitivity of Fermi-LAT to measure this flux around  $5 \times 10^{13} \text{ erg cm}^{-2} \text{s}^{-1}$

# Conclusions

- We have explored for the first time the photon signatures of leptophilic t-channel thermal DM in Cen A, where a DM density spike is believed to have survived to date
- Assuming that the photons measured from the core of Cen A are coming from SM processes, we derive constraints on the DM average annihilation cross section which are 7 orders of magnitude stronger than the ones from measurements of the GC
- The allowed parameter space for our DM candidate is  $40 \text{ GeV} \lesssim m_{\tilde{\chi}} \lesssim 200 \text{ GeV}$  with  $a_R \lesssim 10^{-2}$
- Circular polarised photons, with circular polarisation asymmetries close to 100 %, are expected from DM interactions with the electrons of the AGN jet
- The circular polarised photon signal obtained is not detectable unless a new technique which exploits the circular polarisation fraction is used

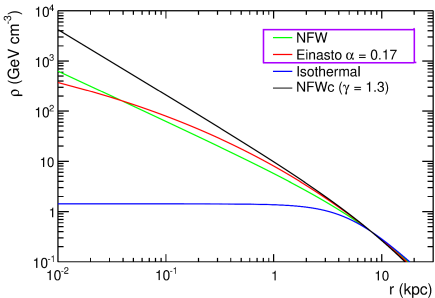
# Backup slides

# DM distribution in the Galaxy

- Well-motivated DM density profiles in our galaxy by the study of rotation curves and N-body simulations *Einasto, Trudy Inst. Astrofiz. Alma-Ata 5 (1965) 87, Navarro, Frenk, White, ApJ 462 (1996) 563, Navarro et al., MNRAS 402 (2010) 21, Ludlow, Angulo MNRAS 465 (2017) L84*

$$\rho_{\text{NFW}}(r) = \rho_s \frac{r_s}{r} \left(1 + \frac{r}{r_s}\right)^2$$
$$\rho_{\text{Ein}}(r) = \rho_s \exp \left\{ -\frac{2}{\alpha} \left[ \left( \frac{r}{r_s} \right)^\alpha - 1 \right] \right\}$$

Profiles	Einasto	NFW
$\rho_s$ ( $\text{GeV cm}^{-3}$ )	0.079	0.307
$r_s$ (kpc)	20.0	21.0
$\alpha_s$	0.17	/



*The Fermi-LAT Collaboration PRD 91 (2015) 122002*

- The local DM density  $\rho_{\chi,0} = 0.385 \pm 0.027 \text{ GeV/cm}^3$  at  $r_\odot = 8.5 \text{ kpc}$  from the Galactic Center (GC) *Catena and Ullio JCAP08 (2010) 004*

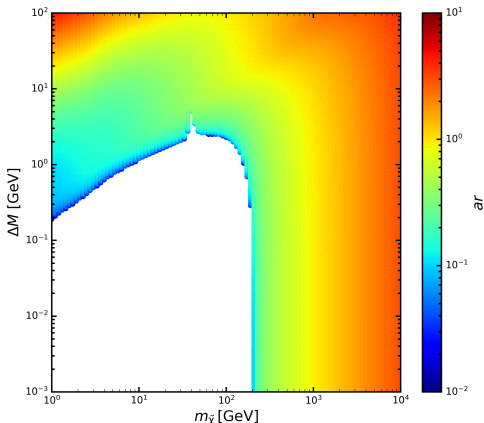
# Relic density

- Thermal DM production,  $(m_{\tilde{\chi}}, \Delta M) \Rightarrow a_R$  that yields  $\Omega_\chi h^2 = 0.120 \pm 0.001$

$$\Omega_\chi h^2 \sim \frac{1}{\sigma v_{eff}}, \quad \sigma v_{eff} = \sigma v_{\tilde{\chi}\tilde{\chi}} + \sigma v_{\tilde{\chi}\varphi} e^{-\frac{\Delta M}{T}} + \sigma v_{\varphi\varphi} e^{-\frac{2\Delta M}{T}},$$

$\sigma v_{\tilde{\chi}\tilde{\chi}} \sim \frac{a_R^4}{m_\chi^2}$ ,  $\sigma v_{\tilde{\chi}\varphi} \sim \frac{a_R^2 g^2}{m_\chi^2}$ ,  $\sigma v_{\varphi\varphi} \sim \frac{g^4}{m_\chi^2}$ , where  $g$  is a gauge coupling

*M. Cermeño, C. Degrande, L. Mantani, Phys.Dark Univ. 34 (2021) 100909*

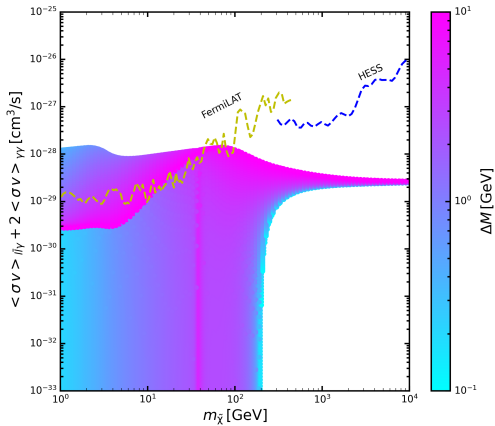


# Indirect detection constraints

- $\tilde{\chi}\tilde{\chi} \rightarrow e^+e^-$  velocity suppressed
- $\tilde{\chi}\tilde{\chi} \rightarrow e^-e^+\gamma$  and  $\tilde{\chi}\tilde{\chi} \rightarrow \gamma\gamma$  relevant channels
- yellow and blue lines are the upper limits from Fermi-LAT and HESS

Ackermann et al., PRD 727 D 91 (2015) 122002, Abdallah et al., PRL 731120 (2018) 201101

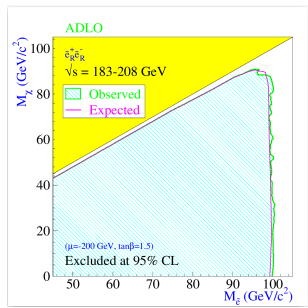
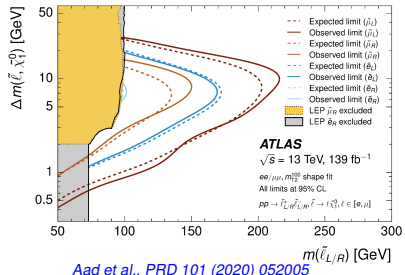
- For  $m_\chi \gtrsim 200$  GeV cases with  $\Delta M < 10^{-1}$  GeV overlap with the rest of the solutions



M. Cermeño, C. Degrande, L. Mantani, Phys.Dark Univ. 34 (2021) 100909

# Collider constraints

- $\varphi$  pair produced through electro-weak interactions
  - Constraints from  $\varphi \rightarrow \tilde{\chi} e^-$ , unless  $\Delta M$  is too small
  - LHC excludes only  $m_\varphi \lesssim 100$  GeV for  $\Delta M \sim$  few GeV
  - LEP constraints evaded  $\frac{m_\varphi}{m_\chi} \leq 1.03$
  - Constraints from mono-photon events at LEP less stringent than the ones from Fermi LAT and HESS
- Kopp, Michaels, Smirnov, JCAP 04 (2014) 022*
- Strongest constraint  $\Rightarrow Z$  width,  $m_\varphi > M_Z/2 = 45$  GeV



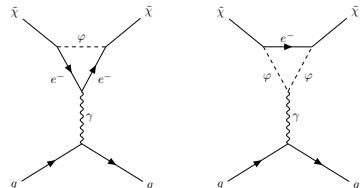
LEP2 SUSY Working Group (2004)

# Direct detection constraints

$$\mathcal{L}_{eff} = \mathcal{A} \bar{\psi}_{\tilde{\chi}} \gamma^\mu \gamma^5 \psi_{\tilde{\chi}} \partial^\nu F_{\mu\nu}$$

$\mathcal{A}$  the anapole form factor

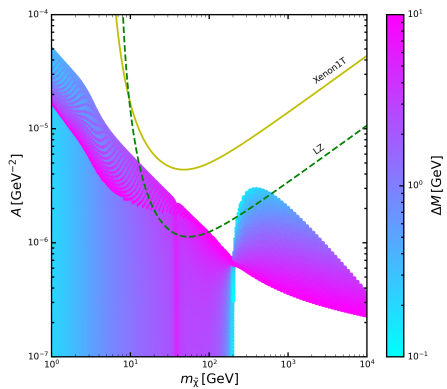
M. Cermeño, C. Degrande, L. Mantani, Phys.Dark Univ. 34 (2021) 100909



- Upper bounds by XENON1T (solid) and the projected LZ (dashed)

Aprile et al., PRL 121 (2018) 111302,

Mount et al., arXiv:1703.09144



# Anapole form factor

Our Majorana DM particle can interact via one loop anapole moment

$$\mathcal{L}_{eff} = \mathcal{A} \bar{\psi}_{\tilde{\chi}} \gamma^\mu \gamma^5 \psi_{\tilde{\chi}} \partial^\nu F_{\mu\nu}.$$

The anapole form factor for  $|q^2| \ll m_e^2$

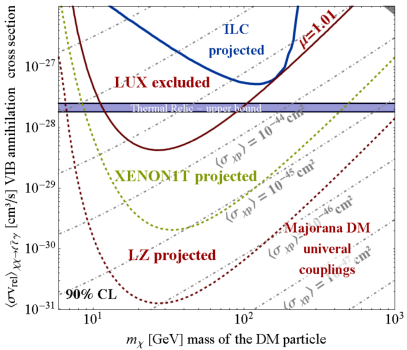
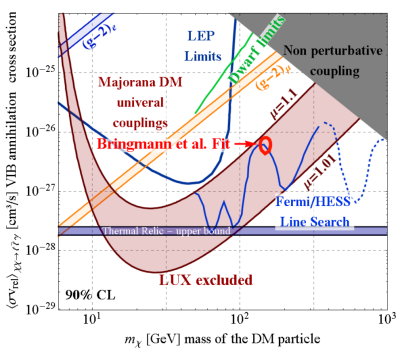
$$\mathcal{A} = -\frac{ea_R^2}{32\pi^2 m_{\tilde{\chi}}^2} \left[ \frac{-10 + 12 \log\left(\frac{\sqrt{|q^2|}}{m_{\tilde{\chi}}}\right) - (3 + 9r^2) \log(r^2 - 1) - (3 - 9r^2) \log r^2}{9(r^2 - 1)} \right]$$

Kopp, Michaels, Smirnov, JCAP 04 (2014) 022, Baker, Thamm, JHEP 10 (2018) 187

- $\sqrt{|q^2|} = \sqrt{2E_r m_T}$  the transferred momentum, where  $E_r \sim \frac{1}{2} m_{\tilde{\chi}} v_{\tilde{\chi}}^2$  is the recoil energy and  $m_T$  the mass of the target of the experiment
- $r = \frac{m_\varphi}{m_{\tilde{\chi}}}$ , for  $r^2 \lesssim 1.001$  the perturbation theory is not valid anymore, need of the next term in the expansion

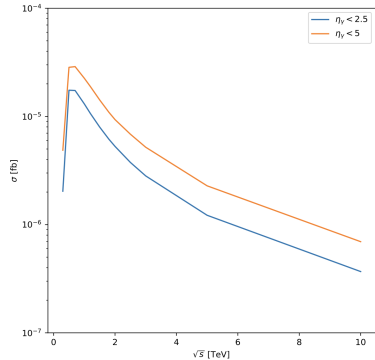
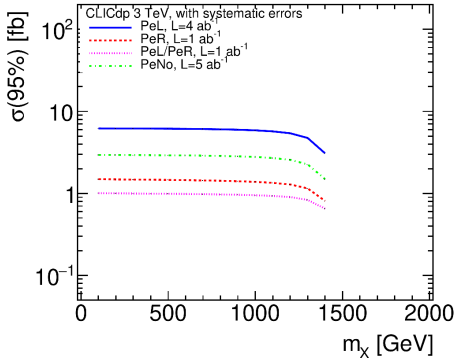
# Mono-photon searches

Mono-photon events coming from  $e^-e^+ \rightarrow \tilde{\chi}\tilde{\chi}\gamma$  at LEP and the future ILC



# Mono-photon searches

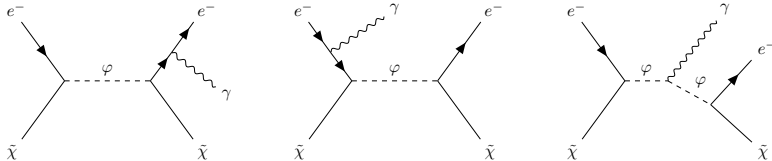
Mono-photon events coming from  $e^-e^+ \rightarrow \tilde{\chi}\tilde{\chi}\gamma$  at CLIC ( $\sqrt{s} = 3$  TeV)



95 % confidence level upper limit cross section expected from CLIC  
VS

cross section for monophoton events for our best fit point  $m_{\tilde{\chi}} = 123$  GeV  $a_R = 0.018$

# Resonances of the process



$p_{\tilde{\chi}} = (m_{\tilde{\chi}}, \vec{0})$ ,  $p_e = (E_e, \vec{p}_e)$  the incoming DM and electron four-momenta,  
 $p'_{\tilde{\chi}} = (E'_{\tilde{\chi}}, \vec{p}'_{\tilde{\chi}})$ ,  $p'_e = (E'_e, \vec{p}'_e)$  the outgoing ones

- Two resonances

$$s = (p_e + p_{\tilde{\chi}})^2 = m_\varphi^2 \Rightarrow E_{R1} = \frac{m_\varphi^2 - m_{\tilde{\chi}}^2}{2m_{\tilde{\chi}}} \approx \Delta M$$

$$s' = (p'_e + p'_{\tilde{\chi}})^2 = m_\varphi^2 \Rightarrow E_{R2} = \frac{m_\varphi^2 - m_{\tilde{\chi}}^2 + 2m_{\tilde{\chi}}E_\gamma}{2(m_{\tilde{\chi}} - E_\gamma(1 - \cos\theta_\gamma))}$$

$\theta_\gamma$  the angle between the emitted photon and the incoming CR electron

# Resonances of the process

When the minimum electron energy

$$E_{\min} = \frac{E_\gamma}{1 - \frac{E_\gamma}{m_{\tilde{\chi}}} \cos \theta_\gamma}$$

is higher than  $E_{R1}$ ,

$$E_\gamma > \frac{m_{\tilde{\chi}}(m_\varphi^2 - m_{\tilde{\chi}}^2)}{2m_{\tilde{\chi}}^2 + (m_\varphi^2 - m_{\tilde{\chi}}^2)(1 - \cos \theta_\gamma)}$$

the first resonance cannot happen anymore.

The drop-off between  $E_{\gamma,1} = \frac{m_{\tilde{\chi}}(m_\varphi^2 - m_{\tilde{\chi}}^2)}{2m_\varphi^2}$  and  $E_{\gamma,2} = \frac{(m_\varphi^2 - m_{\tilde{\chi}}^2)}{2m_{\tilde{\chi}}}$ .

For  $\Delta M \ll m_\varphi \sim m_{\tilde{\chi}} \Rightarrow E_{\gamma,1} \sim E_{\gamma,2} \sim \Delta M$ .

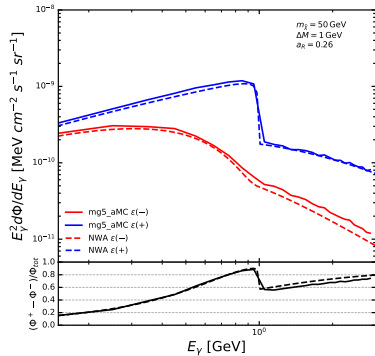
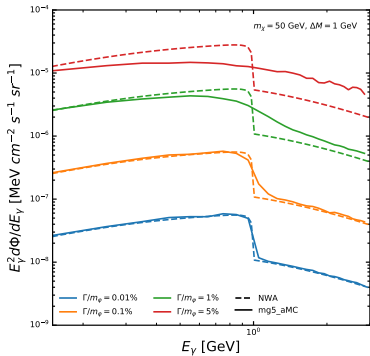
Beyond this energy, only the second resonance contributes to the flux.

# The Narrow Width Approximation

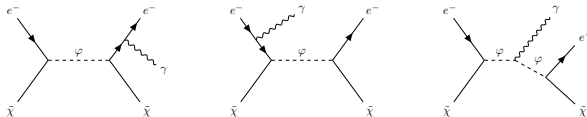
- We are interested in cases with  $\Delta M \ll m_\varphi$
- the total width of the mediator is

$$\Gamma_{\text{tot}} \sim \Gamma_{\varphi \rightarrow e^-\bar{\chi}} = \frac{1}{8\pi} a_R^2 \frac{(m_\varphi^2 - m_{\bar{\chi}}^2)^2}{2m_\varphi^3} \approx \frac{1}{4\pi} a_R^2 \frac{(\Delta M)^2}{m_\varphi}$$

- $\frac{\Gamma_{\text{tot}}}{m_\varphi} \propto \left(\frac{\Delta M}{m_\varphi}\right)^2 \ll 1 \Rightarrow \text{NWA}$



# The Narrow Width Approximation



$$\frac{d\tilde{\Phi}_{e\tilde{\chi},\pm}}{dE_\gamma} \equiv \frac{m_{\tilde{\chi}}}{\bar{J}} \frac{d\Phi_{e\tilde{\chi},\pm}}{dE_\gamma} = \int dE_e \frac{d\phi}{dE_e} \frac{d\sigma_\pm}{dE_\gamma}(E_e, E_\gamma),$$

$$\frac{d\tilde{\Phi}_{e\tilde{\chi},\pm}}{dE_\gamma} = \int \frac{d\phi}{dE_e} \frac{d\tilde{\sigma}_{1\pm}}{dE_\gamma} dE_e + \int \frac{d\phi}{dE_e} \frac{d\tilde{\sigma}_{2\pm}}{dE_\gamma} dE_e,$$

the differential cross section for the first diagram

$$\frac{d\tilde{\sigma}_{1\pm}}{dE_\gamma} = \sigma_{e^-\tilde{\chi}\rightarrow\varphi}(E_e) \frac{d\Gamma_{\varphi\rightarrow e^-\tilde{\chi}\gamma^\pm}}{dE_\gamma}(E_\gamma) \frac{1}{\Gamma_{\text{tot}}}$$

the differential cross section for the other two

$$\frac{d\tilde{\sigma}_{2\pm}}{dE_\gamma} = \frac{d\sigma_{e^-\tilde{\chi}\rightarrow\varphi\gamma^\pm}}{dE_\gamma}(E_e, E_\gamma) \frac{\Gamma_{\varphi\rightarrow e^-\tilde{\chi}}}{\Gamma_{\text{tot}}}$$

with  $\Gamma_{\text{tot}} = \Gamma_{\varphi\rightarrow e^-\tilde{\chi}} + \Gamma_{\varphi\rightarrow e^-\tilde{\chi}\gamma^\pm}$

# DM density spike formation

Assumptions taken

- Adiabatic growth
- Collisionless DM
- Cuspy initial profile
- Growth in the center of the DM halo
- The DM halo did not undergo a merger

The spike is expected to smooth down because of dynamical relaxation due to the scattering of DM with stars if the relaxation time is smaller than the age of the Universe, i.e.,

$$t_r \sim 2 \cdot 10^9 \text{ yr} \left( \frac{M_{\text{BH}}}{4.3 \cdot 10^6 M_{\odot}} \right) < H_0^{-1} \sim 10^{10} \text{ yr}$$

- For the MW  $t_r \sim 2 \text{ Gyr}$
- For Cen A  $t_r \sim 10^2 \text{ Gyr}$

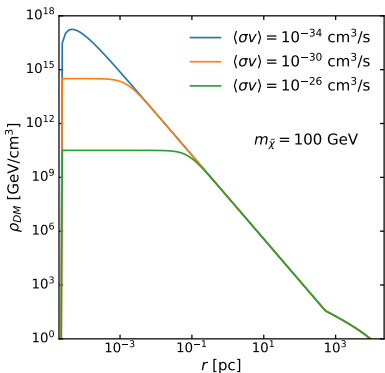
# DM density in Cen A

$$\rho_{DM}(r) = \begin{cases} 0 & r < 4R_S \\ \frac{\rho_{sp}(r)\rho_{sat}}{\rho_{sp}(r)+\rho_{sat}} & 4R_S \leq r < R_{sp}, \\ \rho_0 \left(\frac{r}{r_0}\right)^{-1} \left(1 + \frac{r}{r_0}\right)^{-2} & r \geq R_{sp} \end{cases}$$

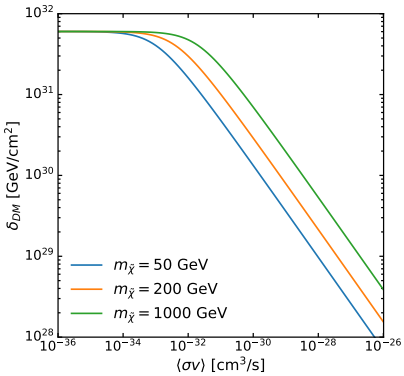
$\delta_{DM} \equiv \int_{4R_S}^{r_0} \rho_{DM}(r) dr$

$$\rho_{sp}(r) = \rho_0 \left(\frac{R_{sp}}{r_0}\right)^{-1} \left(1 - \frac{4R_S}{r}\right)^3 \left(\frac{R_{sp}}{r}\right)^{7/3}, \quad \rho_{sat} \simeq \frac{m_\chi}{\langle\sigma v\rangle t_{BH}}$$

with  $R_S = 5 \times 10^{-6}$  pc,  $r_0 = 20$  kpc,  $\rho_0 \sim 1$  GeV/cm<sup>3</sup>,  $R_{sp} = 10^8 R_S$



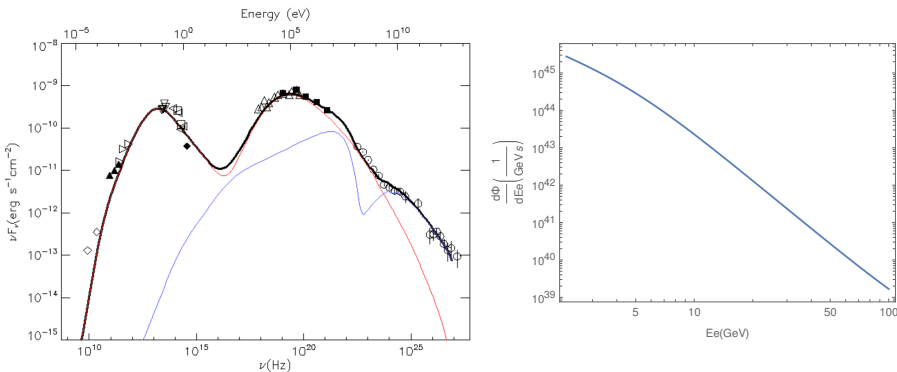
$m_{\tilde{\chi}} = 100$  GeV



# The electron energy spectrum in the jet

Assuming that the gamma-ray photons coming from the Cen A core are due to synchrotron self-Compton radiation from two emitting zones (both located at  $\theta_0 = 30^\circ$  with respect to the line of sight), the electron energy spectrum can be derived [Abdalla et al., A & A 619 \(2018\) A71](#)

At least part of the photon emission at  $E_\gamma > 300$  GeV arises on large scales [Abdalla et al., Nature 582 \(2020\) 356](#)



We use this photon flux as our background to measure the signals and to put constraints

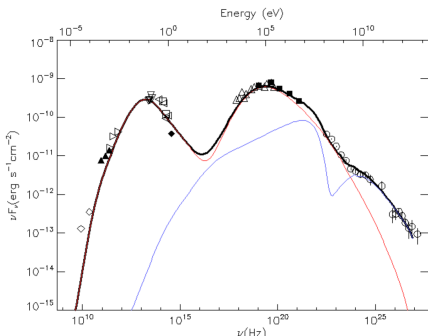
# The electron energy spectrum in the jet

Assuming that the gamma-ray photons coming from the Cen A core are due to synchrotron self-Compton (SSC) the electron energy spectrum can be derived [Abdalla et al., A & A 619 \(2018\) A71](#)

$$\frac{1}{d^2_{\text{AGN}}} \frac{d\Phi_e^{\text{AGN}}}{dE_e} = \frac{1}{d^2_{\text{AGN}} m_e} \int_{0.9}^1 \frac{d\mu}{\Gamma_B(1-\beta_B\mu)} \frac{d\Phi_e^{\text{AGN}}}{d\gamma}$$

$$\frac{d\Phi_e}{d\gamma}^{\text{AGN}} = \frac{1}{2} k_e [\gamma \Gamma_B (1 - \beta_B \mu)]^{-s_1} \left[ 1 + \left( \gamma (\Gamma_B (1 - \beta_B \mu)) / \gamma'_{br} \right)^{s_2 - s_1} \right]^{-1}$$

$$\Gamma_B = (1 - \beta_B^2)^{-\frac{1}{2}} \sim 7, \quad \delta = [\Gamma_B (1 - \beta_B \cos \theta_0)]^{-1}, \quad \gamma_{\min} = \frac{\gamma'_{\min}}{\Gamma_B (1 - \beta_B \mu)}, \quad \gamma_{\max} = \frac{\gamma'_{\max}}{\Gamma_B (1 - \beta_B \mu)}$$

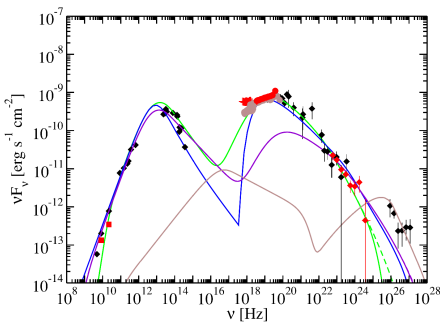


Parameter	the 1st SSC zone	the 2nd SSC zone
$\delta$	1.0	1.0
$\theta_0$	30°	30°
B (G)	6.2	17.0
$R_b$ (cm)	$3.0 \times 10^{15}$	$8.8 \times 10^{13}$
$s_1$	1.8	1.5
$s_2$	4.3	2.5
$\gamma'_{\min}$	$3 \times 10^2$	$1.5 \times 10^3$
$\gamma'_{\max}$	$1 \times 10^7$	$1 \times 10^7$
$\gamma'_{brk}$	$8.0 \times 10^2$	$3.2 \times 10^4$
$L_e$ (erg s <sup>-1</sup> )	$3.1 \times 10^{43}$	$3 \times 10^{40}$

$$L_e = \int_{-1}^1 \frac{d\mu}{\Gamma_B(1-\beta_B\mu)} \int_{\gamma_{\min}}^{\gamma_{\max}} dy m_e \gamma \frac{d\Phi_e^{\text{AGN}}}{d\gamma} [\gamma (\Gamma_B (1 - \beta_B \mu))]$$

# The electron energy spectrum in the jet: other works

Other works as [Gorchtein, Profumo, Ubaldi, PRD 82 \(2010\) 083514](#), [Huang, Rajaraman, and Tait, JCAP 05 \(2012\) 027](#), [Gómez, Jackson, Shaughnessy, PRD 88 \(2013\) 015024](#) used the fit from [Abdo et al., ApJ 719 \(2010\) 1433 \(2010\)](#) taking  $L_e = 10^{45}$  erg/s (Eddington limit)



Parameter	Symbol	Green <sup>1</sup>	Blue <sup>2</sup>	Violet <sup>3</sup>	Brown <sup>4</sup>
Bulk Lorentz factor	$\Gamma_j$	7.0	5 → 2	3.7	2.0
Doppler factor	$\delta_D$	1.0	1.79 → 1.08	3.9	3.1
Jet angle	$\theta$	30°	25°	15°	15°
Magnetic field (G)	$B$	6.2	0.45	0.2	0.02
Variability timescale (s)	$t_v$	$1.0 \times 10^5$		$1 \times 10^5$	$1 \times 10^5$
Comoving blob size scale (cm)	$R_b$	$3.0 \times 10^{15}$	$3 \times 10^{15}$	$1.1 \times 10^{16}$	$9.2 \times 10^{15}$
Low-energy electron spectral index	$p_1$	1.8	3.2	1.8	1.8
High-energy electron spectral index	$p_2$	4.3		4.0	3.5
Minimum electron Lorentz factor	$\gamma_{\min}$	$3 \times 10^3$	$1.3 \times 10^3$	$8 \times 10^2$	$8 \times 10^2$
Maximum electron Lorentz factor	$\gamma_{\max}$	$1 \times 10^8$	$1 \times 10^7$	$1 \times 10^8$	$1 \times 10^8$
Break electron Lorentz factor	$\gamma_{\text{bk}}$	$8 \times 10^2$		$2 \times 10^3$	$4 \times 10^5$
Jet power in magnetic field (erg s <sup>-1</sup> )	$P_{j,B}$	$6.5 \times 10^{43}$	$1.7 \times 10^{41}$	$2.7 \times 10^{41}$	$4.3 \times 10^{38}$
Jet power in electrons (erg s <sup>-1</sup> )	$P_{j,e}$	$3.1 \times 10^{43}$	$3.1 \times 10^{42}$	$2.3 \times 10^{42}$	$7.0 \times 10^{40}$

<sup>1</sup> SSC model.

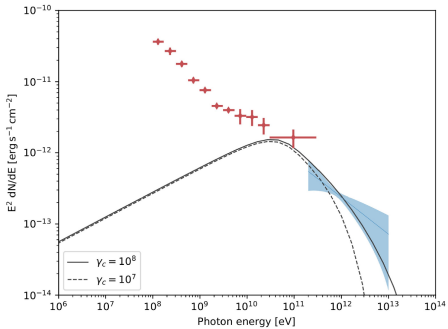
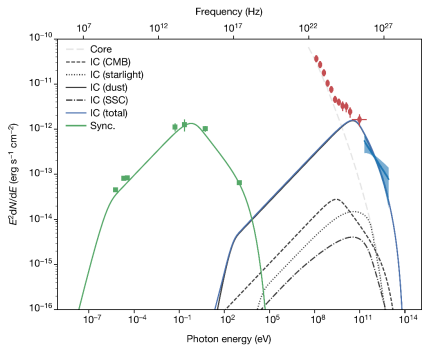
<sup>2</sup> Decelerating Jet model (Georganopoulos & Kazanas 2003).

<sup>3</sup> SSC model excluding X-rays.

<sup>4</sup> SSC Fit to HESS data only.

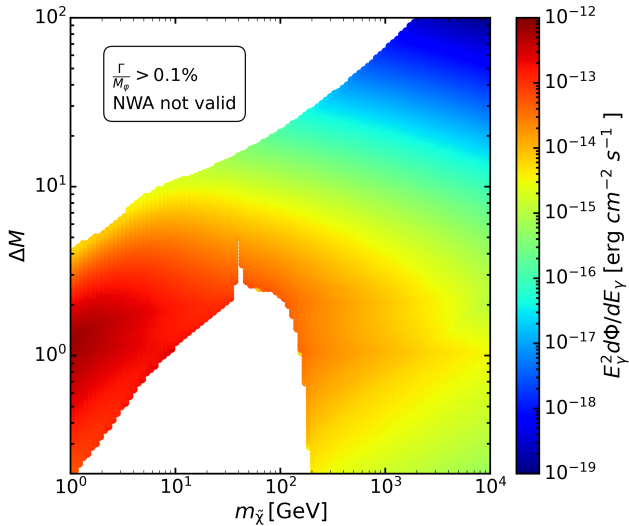
# The electron energy spectrum in the jet: other works

HESS demonstrated the alignment of a substantial part of the very high energy emission with the large-scale radio jet *H. Abdalla et al., Nature 582 (2020) 356*



# Total flux from scattering in the AGN

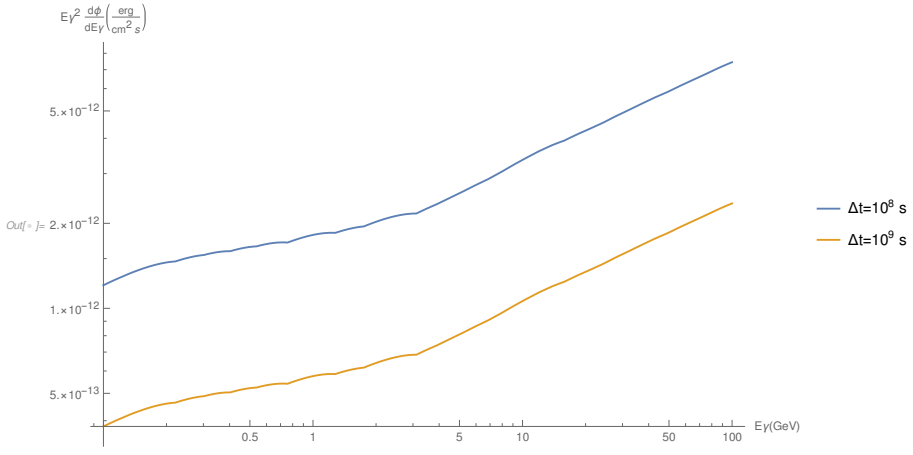
The total flux of photons coming from  $\tilde{\chi}e^- \rightarrow \tilde{\chi}e^-\gamma$  in the AGN jet cannot reach values of the order of the sensitivity of Fermi LAT ( $\sim 5 \cdot 10^{13}$  erg/s) unless  $m_\varphi < 45$  GeV



# Sensitivity Fermi-LAT Cen A

$$\epsilon \sim 0.1, A_{\text{eff}} \sim 10^4 \text{ cm}^2$$

$$\frac{N_{\text{signal}}}{\sqrt{N_{\text{back}}}} \sim 3 \Rightarrow \frac{\frac{d\Phi_{e\chi}}{dE_\gamma}}{\sqrt{\frac{d\Phi_{\text{back}}}{dE_\gamma}}} \sqrt{2\epsilon E_{\gamma, \text{peak}} A_{\text{eff}} \Delta t} = 3$$



# Fit of the Cen A excess

Assuming that the data measured by Fermi-LAT and HESS can be explained only partially with known astrophysical sources, we fit energies below 2.4 GeV and above 300 GeV with a broken power law

$$\frac{d\Phi^{back}}{dE_\gamma} = \begin{cases} kE_\gamma^{-\gamma_1} & E_\gamma \leq E_{br} \\ kE_{br}^{\gamma_2+\gamma_1} E_\gamma^{-\gamma_2} & E_\gamma > E_{br} \end{cases}$$

where  $E_{br} = 2.4$  GeV and fit the remaining data with DM annihilation.

The total flux expression that we fit is therefore given by  $\frac{d\Phi}{dE_\gamma} = \frac{d\Phi^{back}}{dE_\gamma} + \frac{d\Phi^{ann}}{dE_\gamma}$ .

The annihilation flux  $\frac{d\Phi^{ann}}{dE_\gamma} = \int_0^\infty dE'_\gamma K(E_\gamma, E'_\gamma) \frac{d\Phi^{ann}}{dE'_\gamma}(E'_\gamma)$ , where  $K(E_\gamma, E'_\gamma) = \frac{1}{\sqrt{2\pi}\sigma} e^{-\frac{(E_\gamma - E'_\gamma)^2}{2\sigma^2}}$  with 10 % uncertainty at the experimental level  $\sigma = 0.1E'_\gamma$ .

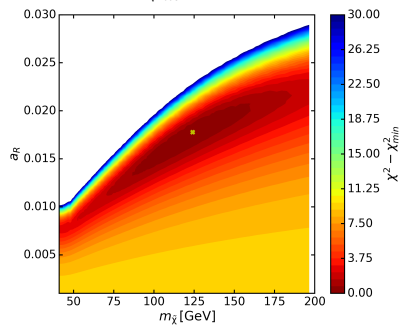
$\{k, \gamma_1, \gamma_2, a_R, m_{\tilde{\chi}}\}$  free parameters

$$N_{data} = 19, N_{dof} = 19 - 5 = 14$$

$$\chi^2 = \sum_{i=0}^{N_{data}} \frac{(O_{meas}^i - O_{th}^i)^2}{\sigma_i^2}$$

$O_{meas}^i$  the measured values,  $O_{th}^i$  the theoretical prediction and  $\sigma_i$  the uncertainty of the data

Best fit  $m_{\tilde{\chi}} = 123$  GeV,  $\Delta M = 2$  GeV and  $a_R = 0.018$   
with  $\chi^2_{min} = 1.59$  and  $\chi^2_{min,back} = 13.65$



# Fit of the Cen A photon excess with DM annihilation

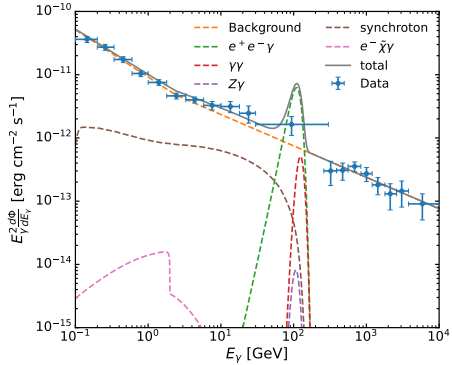
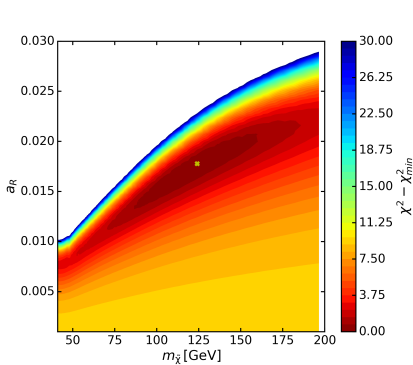
- We fit energies below 2.4 GeV and above 300 GeV with a broken power law

$$\frac{d\Phi^{back}}{dE_\gamma} = \begin{cases} kE_\gamma^{-\gamma_1} & E_\gamma \leq E_{br} \\ kE_{br}^{\gamma_2+\gamma_1} E_\gamma^{-\gamma_2} & E_\gamma > E_{br} \end{cases}$$

where  $E_{br} = 2.4$  GeV, and the remaining data with DM annihilation

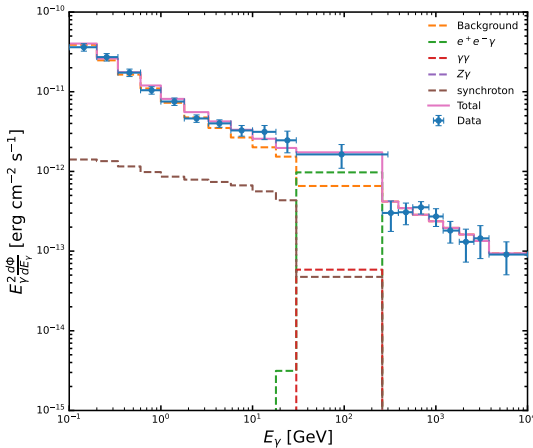
- Total flux  $\frac{d\Phi}{dE_\gamma} = \frac{d\Phi^{back}}{dE_\gamma} + \frac{d\Phi^{ann}}{dE_\gamma}$
- Best fit value for  $m_{\tilde{\chi}} = 123$  GeV,  $\Delta M = 2$  GeV and  $a_R = 0.018$  ( $\chi^2_{min} = 1.59$ )

M. Cermeño, C. Degrande, L. Mantani, PRD 105 (2022) 8, 083019, arXiv: 2201.07247



# Fit of the Cen A excess binned

- The fit is performed by computing the differential binned flux, i.e. the integral of the differential flux in each bin divided by the bin width
- Best fit for  $m_{\tilde{\chi}} = 123$  GeV,  $\Delta M = 2$  GeV and  $a_R = 0.018$



# Synchrotron radiation

- Synchrotron radiation of the electrons from  $\tilde{\chi}\tilde{\chi} \rightarrow e^- e^+ \gamma$  in the presence of a magnetic field
- Equipartition magnetic field model [Regis, Ullio, PRD 78 \(2008\) 043505](#), [Lacroix, Boehm, Silk, PRD 92 \(2015\) 043510](#)

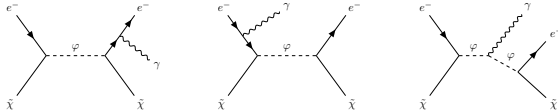
$$B(r) = \begin{cases} B_0 \left( \frac{r}{r_{\text{acc}}} \right)^2 \left( \frac{r}{r_{\text{acc}}} \right)^{-\frac{5}{4}} & r < r_{\text{acc}} \\ B_0 \left( \frac{r}{r_c} \right)^{-2} & r_{\text{acc}} \leq r < r_c \\ B_0 & r \geq r_c, \end{cases}$$

- $B_0 \sim 200 \mu\text{G}$ , obtained for a mean comoving magnetic field of  $B \sim 10 \text{ G}$
- $r_{\text{acc}} = 2GM_{\text{BH}}/\nu_{\text{flow}}^2$  accretion radius,  $\nu_{\text{flow}} \sim 500 - 700 \text{ km/s}$  the velocity of the Galactic wind at the center of Cen A, and  $r_c \sim 5 \text{ kpc}$  the size of the inner radio lobes
- The photon flux coming from the synchrotron radiation

$$E_\gamma^2 \frac{d\Phi_{\text{syn}}}{dE_\gamma} = \frac{8\pi E_\gamma}{d_{\text{AGN}}^2} \int_{4R_S}^{r_0} r^2 dr \int_{E_\gamma}^{m_\chi} dEP(r, E, E_\gamma) \psi_e(r, E)$$

- The electron and positron energy spectrum  $\psi_e(r, E) = \frac{1}{2b(r, E)} \left( \frac{\rho_{DM}(r)}{m_{DM}} \right)^2 \int_E^{m_{DM}} dE_S \frac{d\sigma v_{e^- e^+ \gamma}}{dE_S}$
- $b(r, E) = \frac{4}{3} \sigma_T \frac{B(r)^2}{2\mu_0} \gamma_L^2$  the total energy loss rate,  $\gamma_L = \frac{E}{m_e}$
- The synchrotron emission spectrum  $P(r, E, E_\gamma) = \frac{1}{4\pi e_0} \frac{\sqrt{3}e^3 B(r)}{m_e} G_i \left( \frac{E_\gamma}{E_\gamma^c(r, E)} \right)$
- $G_i(x) = \frac{1}{2} \int_0^\pi G \left( \frac{x}{\sin \alpha} \right) \sin^2 \alpha d\alpha$  the isotropic synchrotron spectrum,  $E_\gamma^c(r, E) = \frac{3eE^2 B(r)}{4\pi m_e^3}$  critical photon energy,  $G(t) = t \int_t^\infty K_{5/3}(u) du$ , where  $K_{5/3}$  is the modified Bessel function of order 5/3

# Circular polarised photon flux from the GC



M. Cermeño, C. Degrande, L. Mantani, Phys.Dark Univ. 34 (2021) 100909

$$\frac{d\Phi_{e\chi,pol}}{dE_\gamma} = \frac{\bar{J}(\Delta\Omega_{\text{obs}})}{m_{\tilde{\chi}}} \int dE_e \frac{d\phi}{dE_e} \left| \frac{d\sigma_+}{dE_\gamma}(E_e, E_\gamma) - \frac{d\sigma_-}{dE_\gamma}(E_e, E_\gamma) \right|$$

- $\bar{J}(\Delta\Omega_{\text{obs}}) = \frac{2\pi}{\Delta\Omega_{\text{obs}}} \int_0^{\theta_{\text{obs}}} d\theta \sin\theta \int_0^{2r_\odot} ds \rho(r(s, \theta)) f(r(s, \theta))$   
 $f(r) = e^{-\frac{(r-r_\odot)}{r_0}}$  the spatial distribution of CR electrons,  $r_0 = 4$  kpc

Strong et al., A&A, 422 (2004) L47

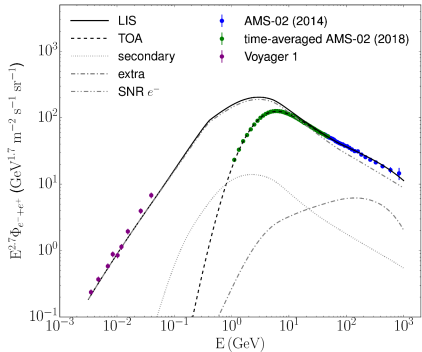
$\rho(r(s, \theta))$  the DM density profile

- $\frac{d\sigma_\pm}{dE_\gamma}(E_e, E_\gamma)$  the differential cross section for  $e^- \tilde{\chi} \rightarrow e^- \tilde{\chi} \gamma_\pm$ , with  $E_e$  the incoming electron energy,  $m_{\tilde{\chi}}$  the DM mass and  $E_\gamma$  the photon energy
- $\frac{d\phi}{dE_e}$  the CR electron energy spectrum in units of  $\text{GeV}^{-1} \text{cm}^{-2} \text{s}^{-1} \text{sr}^{-1}$

# CR electron energy spectrum

The local interstellar spectrum (LIS)

$$\begin{aligned} E_e^{-1.2} & \text{ for } E_e < 0.05 \text{ GeV}, \\ E_e^{-2} & \text{ for } 0.05 \text{ GeV} \lesssim E_e \lesssim 4 \text{ GeV}, \\ E_e^{-3} & \text{ for } E_e > 4 \text{ GeV}. \end{aligned}$$



Injected spectrum

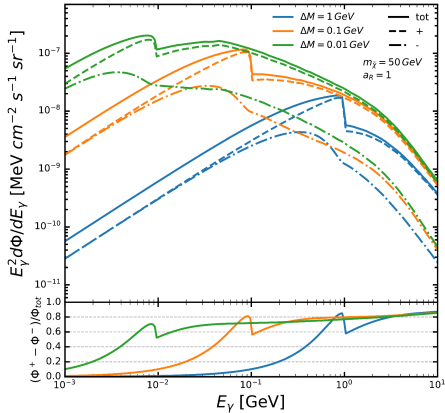
$$\frac{d\Phi_{\text{inj}}}{dE_e} = \begin{cases} k_{e,\text{inj}} \left( \frac{E_e}{\text{GeV}} \right)^{-2.13} & \text{for } E_e \leq 0.109 \text{ GeV} \\ \frac{k_{e,\text{inj}}}{8.9 \cdot 10^{-3}} \left( \frac{E_e}{0.109 \text{ GeV}} \right)^{-2.57} & \text{for } E_e > 0.109 \text{ GeV} \end{cases}$$

with  $k_{e,\text{inj}} = 6.98 \cdot 10^{-3} \text{ GeV}^{-1} \text{ cm}^{-2} \text{ s}^{-1} \text{ sr}^{-1}$ .

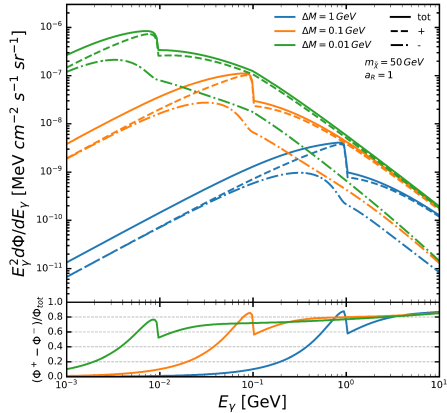
Vittino et al., PRD 100 (2019) 043007

# Photon flux and circular polarisation GC

LIS  $E_e^{-1.2}$  for  $E_e < 0.05 \text{ GeV}$   
 $E_e^{-2}$  for  $0.05 \text{ GeV} \lesssim E_e \lesssim 4 \text{ GeV}$



Injected  $E_e^{-2.13}$  for  $E_e \leq 0.109 \text{ GeV}$   
 $E_e^{-2.57}$  for  $E_e > 0.109 \text{ GeV}$



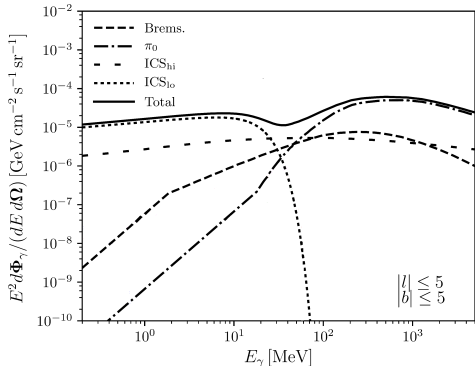
M. Cermeño, C. Degrande, L. Mantani, Phys. Dark Univ. 34 (2021) 100909

$$\frac{\Phi^+ - \Phi^-}{\Phi_{\text{tot}}} \equiv \frac{\frac{d\Phi_{e\tilde{\chi},\text{pol}}}{dE_\gamma}}{\frac{d\Phi_{e\tilde{\chi}}}{dE_\gamma}}, \quad \frac{d\Phi_{e\tilde{\chi},\text{pol}}}{dE_\gamma} = \frac{d\Phi_{e\tilde{\chi},+}}{dE_\gamma} - \frac{d\Phi_{e\tilde{\chi},-}}{dE_\gamma}$$

Asymmetries up to 90 %  
 Flux scales as  $a_R^2/m_\chi^2$

# Prospects of detection for the GC

- Standard circular polarisation: synchrotron emission and curvature radiation
- Gamma-rays from the GC: ICS, bremsstrahlung and inelastic collisions of high energy CRs with the ambient medium
- $E_\gamma^2 \frac{d\phi_{\text{back}}}{dE_\gamma} \sim 10^{-2} \frac{\text{MeV}}{\text{cm}^2 \text{s sr}}$
- $\frac{N_{\text{signal}}}{\sqrt{N_{\text{back}}}} \sim 3 \Rightarrow E_\gamma^2 \frac{d\Phi_{\text{ex}}}{dE_\gamma} \sim 10^{-5} \text{ MeV cm}^{-2} \text{ s}^{-1} \text{ sr}^{-1}, \Delta t \sim 10^8 \text{ s}$  (e-ASTROGAM)
- Detectable fluxes for  $m_\chi \sim 5 \text{ GeV}$
- Different source of electrons?  $\Rightarrow$  AGN



Adapted from [Bartels, Gaggero, Weniger, JCAP05 \(2017\) 001](#)

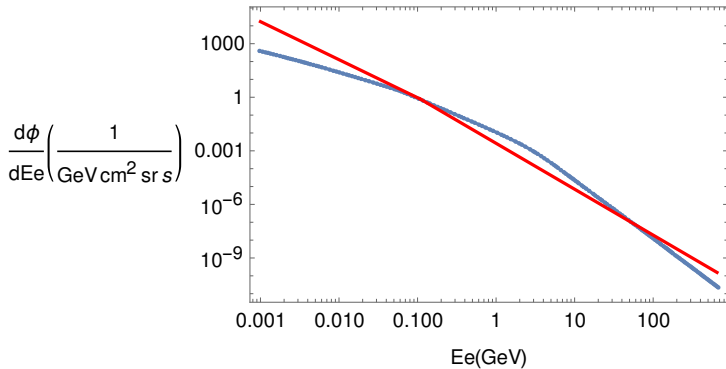
# CR electron energy spectrum GC

The local interstellar spectrum (LIS)

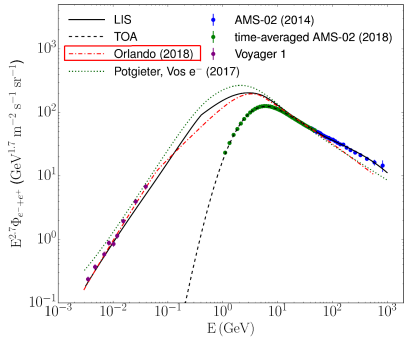
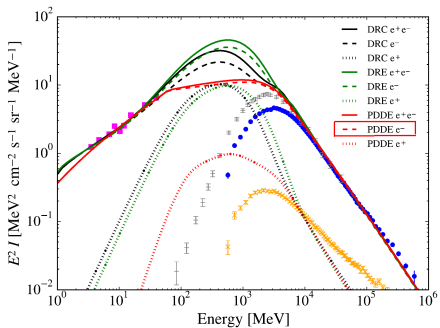
$$\begin{aligned} E_e^{-1.2} & \text{ for } E_e < 0.05 \text{ GeV}, \\ E_e^{-2} & \text{ for } 0.05 \text{ GeV} \lesssim E_e \lesssim 4 \text{ GeV}, \\ E_e^{-3} & \text{ for } E_e > 4 \text{ GeV}. \end{aligned}$$

Injected spectrum

$$\frac{d\Phi_{\text{inj}}}{dE_e} = \begin{cases} k_{e,\text{inj}} \left( \frac{E_e}{\text{GeV}} \right)^{-2.13} & \text{for } E_e \leq 0.109 \text{ GeV} \\ \frac{k_{e,\text{inj}}}{8.9 \cdot 10^{-3}} \left( \frac{E_e}{0.109 \text{ GeV}} \right)^{-2.57} & \text{for } E_e > 0.109 \text{ GeV} \end{cases}$$



# CR electron energy spectrum GC



Orlando, MNRAS 475 (2018) 2724

Vittino et al., PRD 100 (2019) 043007

# Scattering vs annihilation GC

The annihilation rate

$$q_{\tilde{\chi}\tilde{\chi}} \sim \langle\sigma v\rangle \frac{\rho_0}{m_{\tilde{\chi}}} \sim \frac{a_R^4 e^2}{(4\pi)^2 m_{\tilde{\chi}}^2} v_{\tilde{\chi}} \frac{\rho_0}{m_{\tilde{\chi}}}$$

The CR scattering rate

$$q_{e\tilde{\chi}} \sim \sigma_{e\tilde{\chi}} E_e \frac{d\phi}{dE_e} \sim \frac{a_R^2 e^2}{4\pi m_{\tilde{\chi}}^2} E_e \frac{d\phi}{dE_e}$$

The ratio

$$\frac{q_{e\tilde{\chi}}}{q_{\tilde{\chi}\tilde{\chi}}} \sim 10^{-6} a_R^{-2} \left( \frac{E_e \frac{d\phi}{dE_e}}{\text{cm}^{-2} \text{s}^{-1}} \right) \left( \frac{m_{\tilde{\chi}}}{\text{GeV}} \right)$$

# Sensitivity e-ASTROGAM GC

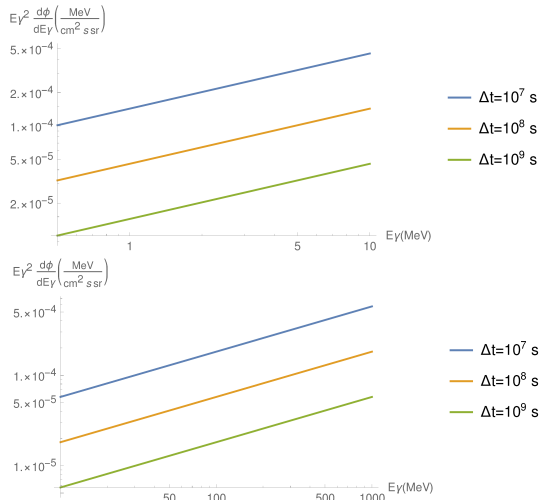
$$\epsilon = 0.013, A_{\text{eff}} = 50 - 560 \text{ cm}^2, E_\gamma = 0.3 - 10 \text{ MeV}$$

$$\epsilon = 0.3, A_{\text{eff}} = 215 - 1810 \text{ cm}^2, E_\gamma = 10 - 3000 \text{ MeV}$$

$$\frac{N_{\text{signal}}}{\sqrt{N_{\text{back}}}} \sim 3$$

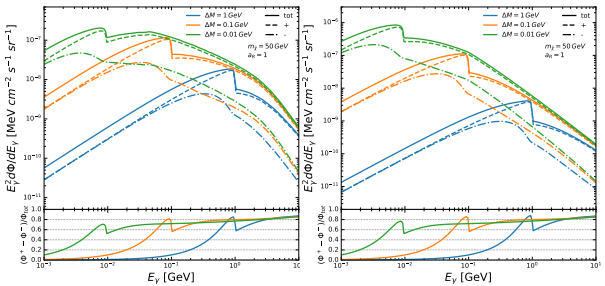
$$\frac{\frac{d\Phi_{e\chi}}{dE_\gamma}}{\sqrt{\frac{d\Phi_{\text{back}}}{dE_\gamma}}} \sqrt{2\epsilon E_{\gamma,\text{peak}} \Delta\Omega A_{\text{eff}} \Delta t} = 3$$

$$E_\gamma^2 \frac{d\phi_{\text{back}}}{dE_\gamma} \sim 10^{-2} \text{ MeV cm}^{-2} \text{ s}^{-1} \text{ sr}^{-1}$$

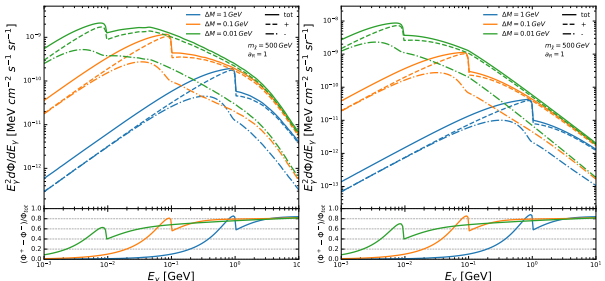


# Results: Photon flux and circular polarisation from the GC

- Left: LIS
- Right: injected spectrum
- Einasto profile,  $\frac{\bar{J}_{\text{NFW}}}{\bar{J}_{\text{Ein}}} \sim 0.7$

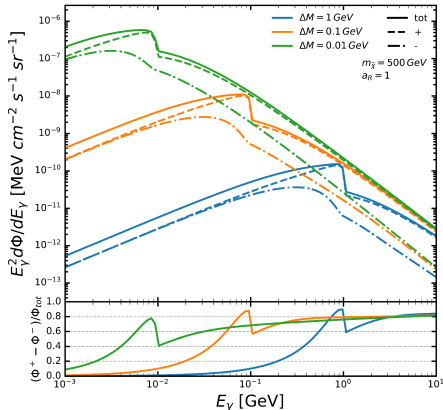
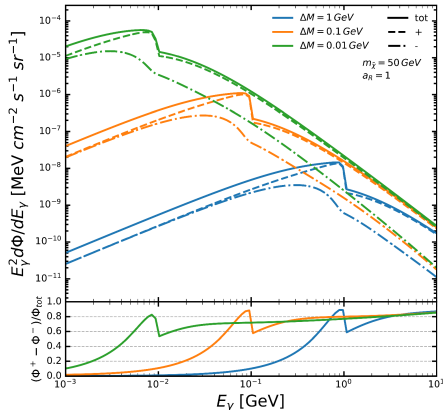


- Thermal relic DM, rescale flux by  $a_R^2$
- $m_{\tilde{\chi}} = 50$  GeV underabundant
- Dirac DM, rescale flux by  $\frac{\rho_{\tilde{\chi}}}{\rho_\chi + \rho_{\tilde{\chi}}}$
- $m_\varphi \geq 45$  GeV cannot be easily evaded



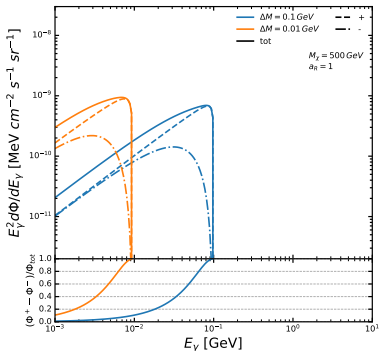
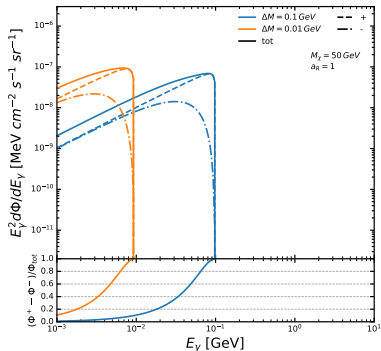
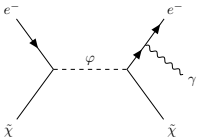
# Results: Photon flux and circular polarisation from the GC

- Energy spectrum  $\frac{d\Phi}{dE_e} = k_e \left( \frac{E_e}{\text{GeV}} \right)^{-3}$ ,  $k_e = 10^{-2} \text{ GeV}^{-1} \text{ cm}^{-2} \text{ s}^{-1} \text{ sr}^{-1}$



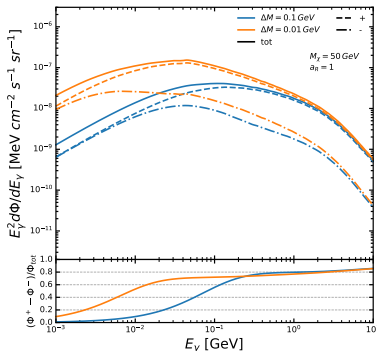
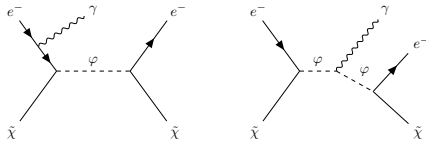
- The electron energy spectrum has a relevant impact on the final results
- Higher circular polarised fluxes could be obtained close to other astrophysical electron sources (AGNs, pulsars, SNRs...)

# Impact of the first resonance on the asymmetry



LIS spectrum

# Impact of the second resonance on the asymmetry



LIS spectrum

